Oral Presentation

The 7th TSME International Conference on Mechanical Engineering
13-16 December 2016

TSME ICOME 2016
Mechanical Engineering Innovation for Green Society

AME0013

Optimal Design of the Inverted GOE 178 Airfoil Profile Rear Spoiler for Student Formula Competition Car

Sutartip Wittayapiyanon and Sathaporn Chuepeng*

Automotive Technology and Alternative Energy Research Group, Department of Mechanical Engineering,
Faculty of Engineering at Sriracha, Kasetsart University Sriracha Campus, 199 Sukhumvit Road, Chonburi 20230, Thailand
* Corresponding Author: E-mail schuepeng@eng.src.ku.ac.th, Telephone Number +6638354580, Fax Number +6638354849

Abstract

A car at speed withstands some forces that generate instability due to yaw, roll, and pitch motions. The center of gravity of a car tends to shift forward when the car speeds up. This brings about greater drag and lift forces. In particular, the latter causes the rear wheels to float off the track and hence, instability. A way to resolve this problem is to generate a counter down force, e.g. by adding a rear spoiler. This work presents the performance characteristics of the rear spoiler intentionally designed for Student Formula competition car. The inverted GOE 178 airfoil profile was simulated using commercial software package ANSYS with other two profiles for comparison and validation. The pitch angles of the profiles were varied from 10 to 60 degrees to the horizontal plane and the simulated velocity of the longitudinal wind were ranging from 60 to 200 km/h ($0.3\times10^6 < Re < 1.0\times10^6$), neglecting other lateral disturbances. The analysis includes pressure, streamline as well as lift and drag forces over the surface of the specimens. With the increasing wind velocity, the drag and lift forces were greater. The more the pitch angles of the spoiler, the more the drag force. The optimum pitch angle design of 40^o for the inverted GOE 178 airfoil profile rear spoiler is obtained over the speed range. The subsequent results derived from this simulation will be used as a design consideration for manufacturing the spoiler which will be properly tested further.

Keywords*:* airfoil; car; drag; simulation; spoiler.

1. Introduction

Vehicles nowadays are progressively developed and relatively capable of running at higher speed than predecessors. At a greater extent of velocity, a car endures some forces, e.g. longitudinal, lateral, etc., generating instability. This brings the changes in drag and lift forces. In particular, the latter causes the rear wheels to float off the track and hence, shakiness. A way to resolve this problem is to generate a counter down force by adding a rear spoiler with various profiles. Symmetrical profiles are conventional while unsymmetrical profiles are gained more attention as they are believed to generate greater down force [1].

One of the most famous symmetrical profiles, a NACA 0012 airfoil has been widely used. Numerous publications explored its flow characteristics. Shoja-Sani *et al*. (2014) [2] investigated aerodynamic characteristics of rarefied flow around NACA 0012 airfoil using Direct Simulation Monte Carlo (DSMC) and Navier–Stokes (NS) solvers. In addition, steady-state NS solutions for the flow over the profile have been investigated by Swanson and Langer (2016) [3]. In terms of application, Bhat and Govardhan (2013) [4] studied stall flutter of the profile at low Reynolds number (*Re*) while Gageik *et al*. (2015) [5] studied for a direct numerical simulation of the transonic flow (*Re* = 500,000) around a NACA 0012 airfoil. The NACA 0012 airfoil was tested at high angles of attack by Rainbird *et al*. (2015) [6] while Katkhaw *et al*. (2014) [7] analyzed heat transfer behavior of other profiles of flat plate having 45^o ellipsoidal dimpled surfaces.

A symmetrical NACA 0015 airfoil profile is also of interest in studying flow characteristics. Siauw *et al*. (2010) [8] investigated transient dynamics of the flow around the airfoil using fluidic vortex generators. For a vortex at wing tip, detached-eddy simulation of NACA 0015 airfoil was performed by Liang and Xue (2014) [9]. Under deep dynamic stall, Šidlof *et al*. (2016) [10] conducted an experiment to explore the low-induced vibration of a pitch–plunge NACA 0015 airfoil.

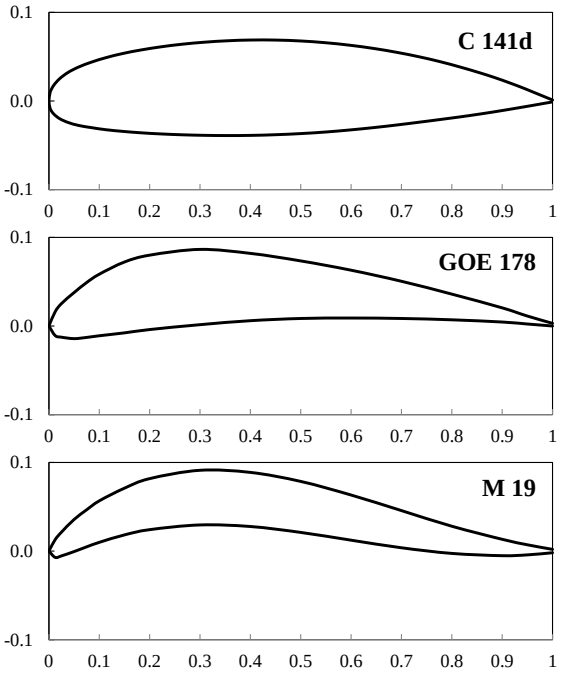

Fig. 1 Unsymmetrical C 141d, GOE 178, and M 19 airfoil profiles [12]

AME0013

Other unsymmetrical airfoil profiles have been extensively used up to present, for example: C 141d, GOE 178 and M 19 [11]. Their unity chord profiles derived from UIUC Applied Aerodynamics Group (2016) [12] are depicted in Fig. 1. This is as their inverted forms in obvious curvature can generate greater down force as per the plots of the lift and drag coefficients shown in Fig. 2, for comparison. All the values were obtained from calculation using values in the database of Drela and Youngren (2013) [13], at zero pitch angle of the airfoils and *Re* = 50,000. In particular, the GOE 178 airfoil profile has been obviously seen in generating high value of lift coefficient and thus, assumingly great down force for its inverted profile. Meanwhile, the GOE 178's drag coefficient is comparatively low among the others.

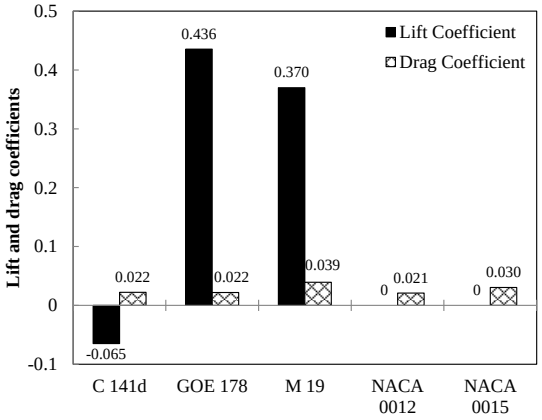

Fig. 2 Comparison of lift and drag coefficients of the airfoil profiles (0^o pitch angle, *Re* = 50,000)

Subsequently, there are some other aspects that have not been studied concerning the air flowing over the inverted GOE 178 airfoil profile. The main aim of this work is to investigate the drag and down forces over the variation in air velocity and the airfoil pitch angle. Analysis of the down force will eventually give some information on suitable pitch angle to be set.

2. Materials and methods

2.1 Governing equations

To focus on the fundamentals of flow and heat transfer of the airfoils, a three-dimensional model is considered. The model was on the assumption of steady-state incompressible turbulent flow. By this conjecture, the continuity, momentum, and energy equations can be listed as [14]:

$$\frac{\partial(\rho)}{\partial t}+\frac{\partial(\rho u_i)}{\partial x_i}+\frac{\partial(\rho v_i)}{\partial y_i}\frac{\partial(\rho w_i)}{\partial z_i}=0 \qquad (1)$$

$$\frac{\partial(\rho u_i)}{\partial t}+\frac{\partial(\rho u_i u_j)}{\partial x_i}=\frac{\partial(P_i)}{\partial x_i}$$
$$+\frac{\partial}{\partial x_i}\left(\mu\left(\frac{\partial u_i}{\partial x_j}+\frac{\partial u_j}{\partial x_i}\right)\right)+\frac{\partial}{\partial x_i}\left(-\rho\overline{u_i' u_j'}\right) \qquad (2)$$

$$\frac{\partial(\rho c_p T)}{\partial t}+\frac{\partial(\rho c_p T u_i)}{\partial x_i}=\frac{\partial}{\partial x_i}\left(\frac{\partial kT}{\partial x_i}\right)+S \qquad (3)$$

where u_i is mean velocity,

u_i' is fluctuating velocity,

ν is kinematic viscosity,

$-\rho\overline{u_i' u_j'}$ is Reynolds-stress tensor,

ρ is fluid density,

μ is dynamics viscosity,

c_p is specific heat, and

T is temperature.

For turbulent flow, linear $k-\varepsilon$ turbulence models of Launder and Sharma (1974) [15] is employed in this work.

The commercial software package ANSYS is used in this study. The governing equations are discretized by the finite volume method, and the second order upwind scheme is adopted for spatial discretization of the convection terms. The segregated solver is used in the simulation, and the SIMPLE algorithm is employed to couple the pressure and velocity [16]. The convergence criteria of iterative solution have been insured when the residual of all variables are less than specific values. The specified value is 10^{-4} for the continuity and momentum equations, and 10^{-6} for the energy equation.

2.2 Spoiler geometry

The two-dimensional models of the inverted airfoils C 141d, GOE 178, and M 19 are displayed in Fig. 3. Meanwhile, the three-dimensional models of all the airfoils are depicted in Fig. 4 with unstructured meshing. The width of all profiles was 1,500 mm. All airfoils used in this work have 280-mm chord and 120% of nose circle thickness.

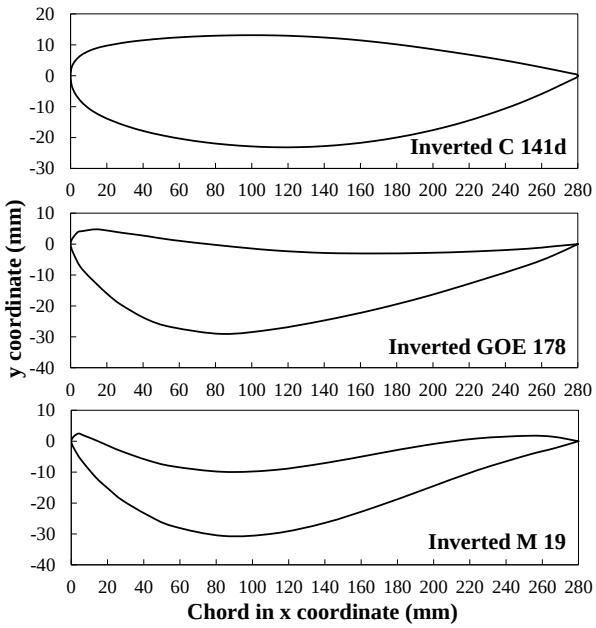

Fig. 3 Two-dimensional models of the unsymmetrical inverted airfoil profiles: C 141d, GOE 178, and M 19 at 0^o pitch angle

2.3 Computational domain

Computational domain and boundary conditions for all the airfoils are depicted in Fig. 5. The x-axis is along to the direction of the drag force while the y-axis is upwards perpendicular to the x-axis, in the direction of the lift force. The air inlet velocities (U_{inlet}) were altered in their vectors in x- and y-axes due to the changes in the pitch angles (α).

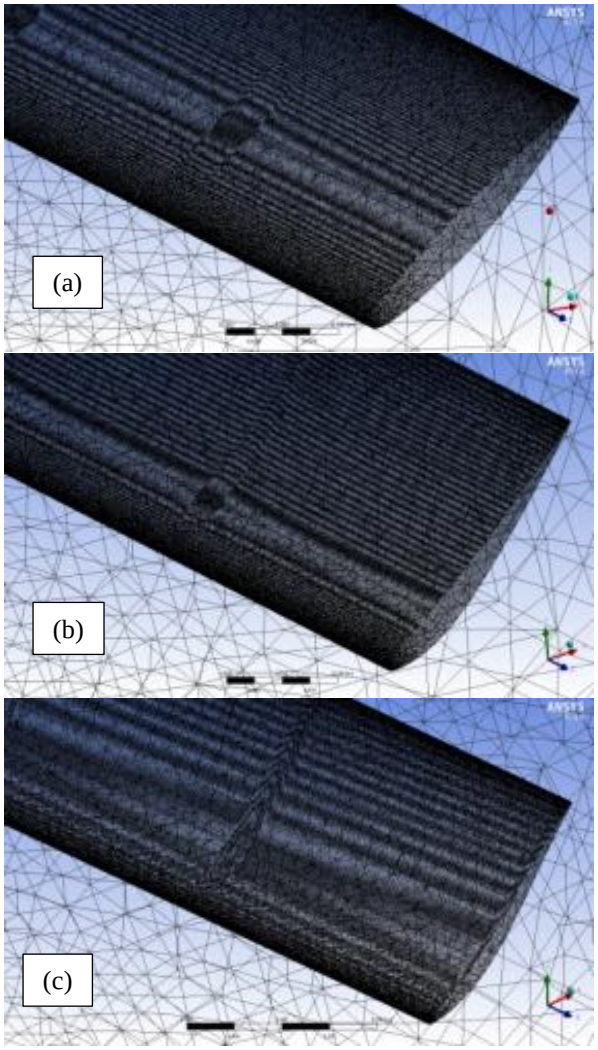

Fig. 4 Three-dimensional models of the inverted airfoil profiles (a) C 141d, (b) GOE 178, and (c) M 19 with unstructured meshing

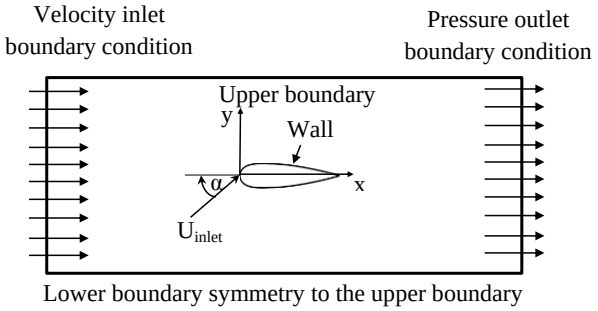

Fig. 5 Two-dimensional computational domain and boundary conditions for the test airfoil profiles

2.4 Reynolds number determination

The velocity range of interest is between 60 km/h and 200 km/h as it is fast enough to observe for distinguishable drag and down force values. This range of velocity causes in resultant Reynolds numbers.

Reynolds number is a dimensionless value that measures the ratio of inertia forces to viscous forces and describes the degree of laminar or turbulent flow. Reynolds number (*Re*) is calculated by [17]

$$Re = \frac{vl}{\nu} \tag{4}$$

where v is air velocity in m/s, l is characteristic length in m, the chord width of the airfoils, and ν is kinematic viscosity of air in m^2/s ($\nu = 1.56\times10^{-5}$ m^2/s at 25°C [18]). The Reynolds number range ($300{,}000 \leq Re \leq 1{,}000{,}000$) corresponding to the velocity range (60 km/h $< v <$ 200 km/h) used in this work is shown in Fig. 6.

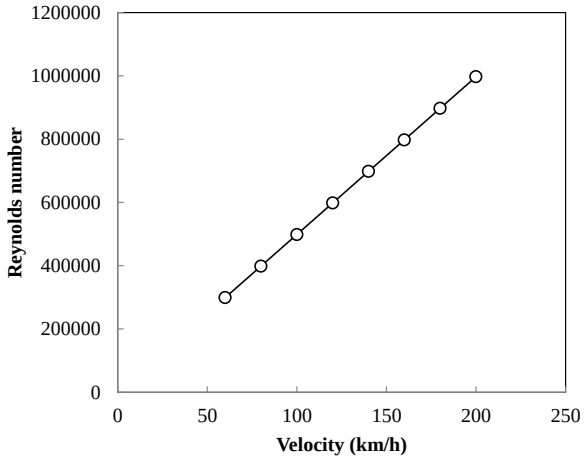

Fig. 6 The Reynolds number and velocity ranges for the drag and down force analysis

3. Results and discussion

3.1 Velocity streamline

The streamlines of velocity over the body of all the inverted airfoil profiles are shown in Fig. 7 at the inlet velocity of 200 km/h with different pitch angles. At low pitch angle, the streamlines behind the airfoil's tails mostly show in order. When the pitch angle of the profiles increased up to 60°, the vortex flow behind the profiles can be obviously seen. Additionally, the point of attack has shown to move up on the profile body at high pitch angle instead of that at low pitch angle (0°).

3.2 Pressure on spoiler

The average pressure values acting on all the inverted airfoil profiles are shown in Fig. 8 at the inlet velocity of 200 km/h as the variation of pitch angles. Note the positive values of pressure indicate the direction to the positive y-axis. By this definition, the negative pressure values represent the direction to the negative y-axis. The more the negative average pressure, the greater the down force.

AME0013

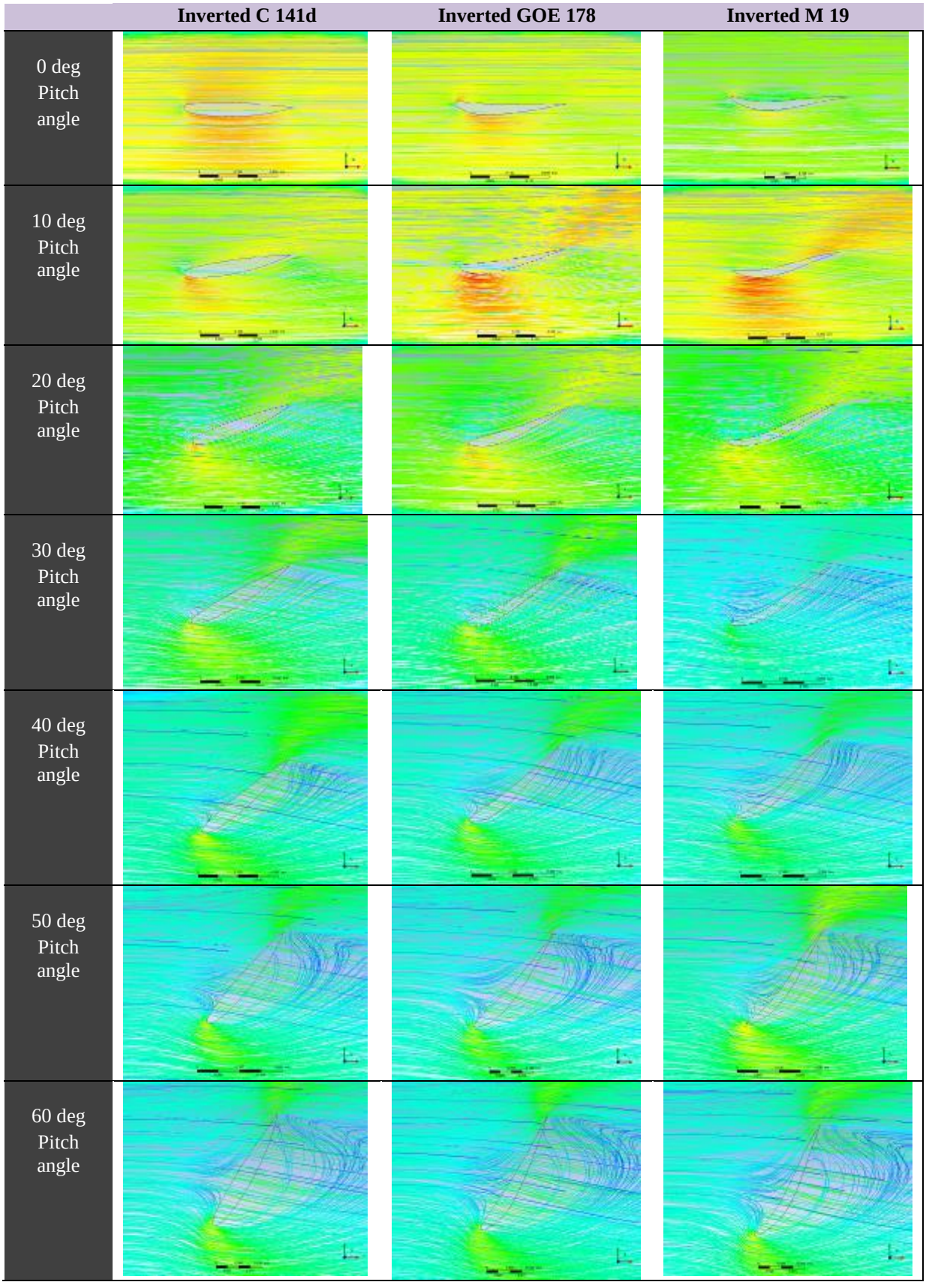

Fig. 7 Velocity streamlines over the inverted C 141d, GOE 178, and M 19 airfoil profiles at 200 km/h for various pitch angles

AME0013

In Fig. 8 at 0° pitch angle, the M 19 airfoil profile apparently generated neutral pressure compared to the other two airfoils that inherently generated positive pressure. Up to 10° pitch angle, all the airfoils produced subtle positive pressure. Afterwards until the pitch angle reaching 60°, the magnitudes of pressure acting on all inverted airfoil profiles increased with those of the inverted GOE 178 showing the greatest extent. By these results, the inverted GOE 178 airfoil profile is considered to be focused on as its capability in generating high pressure on its profile.

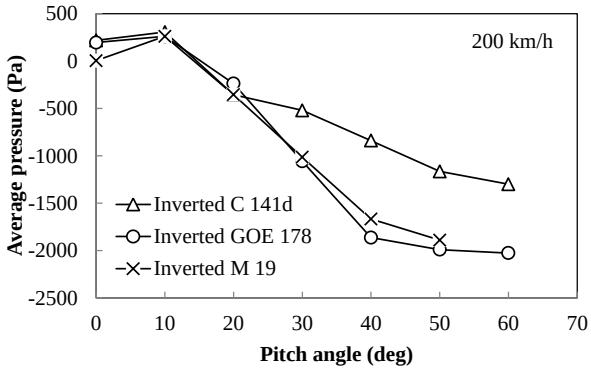

Fig. 8 Average pressure acting on the inverted airfoil profiles at 200 km/h in variation of pitch angle

3.3 Drag and down forces

The drag force acting on the inverted GOE 178 airfoil profile is shown in Fig. 9 as the variation of velocity and pitch angle. The drag forces increased with the increment of velocity. In addition, the steeper pitch angles generated greater drag forces. The highest drag force was by 2,005 N at 60° pitch angle.

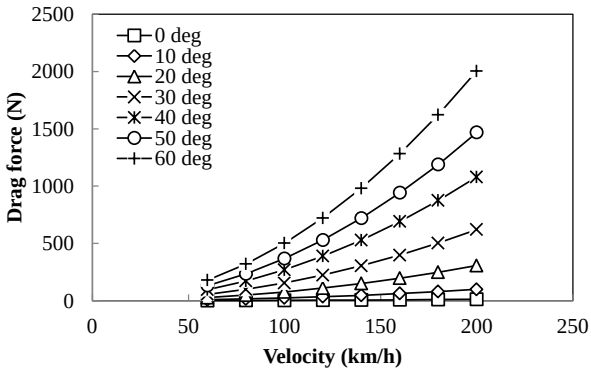

Fig. 9 Drag force acting on the inverted GOE 178 airfoil profile

The magnitudes of down force (negative lift force) acting on the inverted GOE 178 airfoil profile varied with velocity and pitch angle is shown in Fig. 10. Likewise the drag force, the down forces was strengthened when increasing velocity. However, the steeper pitch angles up to 40° generated greater down forces and then the drag forces reclined afterwards. The highest down force was by 1,836 N at 40° pitch angle, 200 km/h. At 60° pitch angle, the drag force was by 1,500 N.

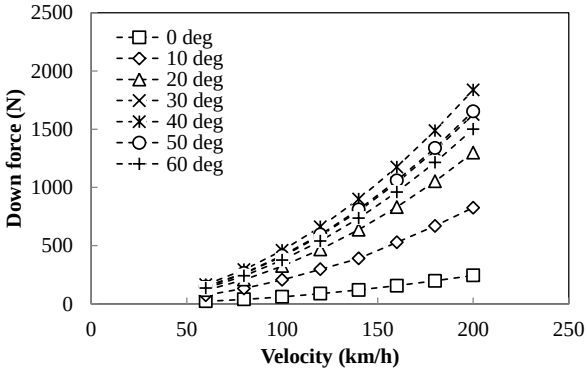

Fig. 10 Down force acting on the inverted GOE 178 airfoil profile

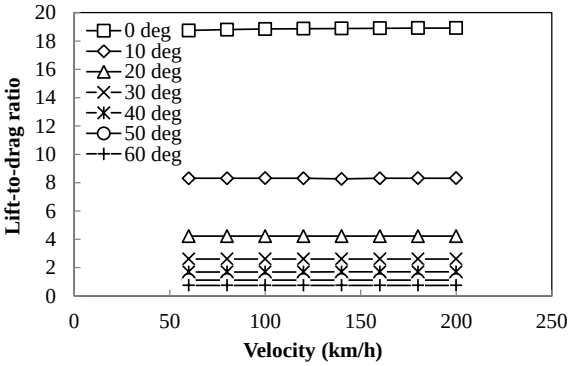

Fig. 11 Lift-to-drag ratio of the inverted GOE 178 airfoil profile

As the variation of velocity and pitch angle, Fig. 11 shows the lift-to-drag ratios of the inverted GOE 178 airfoil profile. The lift-to-drag ratios are shown to be insignificantly dependent on velocity. However, the lift-to-drag ratios are in lowest values for the most inclination of the profile. The maximum and minimum values of the lift-to-drag ratios were by 18.9 and 0.7 for 0° and 60° pitch angles, respectively. At 0° pitch angle, there was very little drag force that resulted in the highest lift-to-drag ratio.

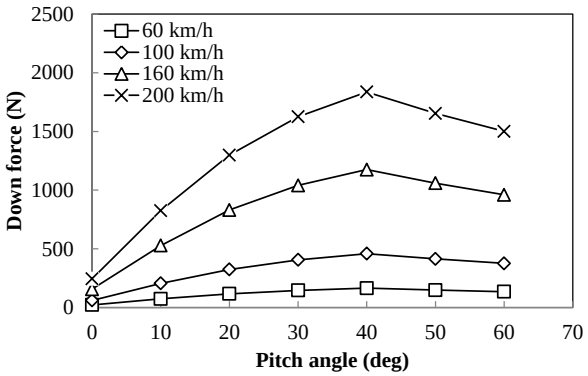

Fig. 12 Down force – pitch angle relationship of the inverted GOE 178 airfoil profile

3.4 Optimum pitch angle

The magnitude plots of down forces in variation of pitch angles of the inverted GOE 178 airfoil profile are shown in Fig. 12. The graphs confirm that the increase in velocity generates greater down forces. The

adjustment of the pitch angles from 0° up to 40° produces the increment of down forces. However, the inclining of the profile over 40° exhibits the reduction in the down forces. For the speed in the range of 60 km/h to 200 km/h, the pitch angle of 40° is apparently seen to be suitable for the competition car in beneficial of down force.

4. Conclusions

The analysis of flow over the inverted GOE 178 airfoil profile as a rear spoiler of a Student Formula competition car using commercial software package ANSYS with comparison of the inverted M 19 and C 141d airfoil profiles can conclude as the followings.

- The steeper pitch angles of all airfoils changed the point of attack on the profile body, created vortex behind the airfoils, and generated different levels of pressure on the profiles.
- The drag force and the down force increased with the increasing velocity. The steeper pitch angles generated greater drag force.
- In the range of 60 km/h to 200 km/h, the 40° pitch angle is beneficial in term of down force for the inverted GOE 178 airfoil profile in the Student Formula competition car.

Careful design of the airfoil profile as a rear spoiler should be taken when the drag force, down force, and pitch angle have to be optimized for power loss that may be concerned in aspect of fuel economy.

5. Acknowledgement

Kasetsart University Faculty of Engineering at Sriracha is acknowledged for financial support to this project (Grant No. STh051330405/0167).

6. References

[1] Haocheng, F., Mingqiang, L., Hu, L. and Zhe, W. (2011). A web-based software framework for aircraft design modeling, analysis and multidisciplinary optimization, *Procedia Environmental Sciences*, vol. 11, pp. 291-296.

[2] Shoja-Sani, A., Roohi, E., Kahrom, M. and Stefanov, S. (2014). Investigation of aerodynamic characteristics of rarefied flow around NACA 0012 airfoil using DSMC and NS solvers, *European Journal of Mechanics - B/Fluids*, vol. 48, pp. 59-74.

[3] Swanson, R.C. and Langer, S. (2016). Steady-state laminar flow solutions for NACA 0012 airfoil, *Computers and Fluids*, vol. 126, pp. 102-128.

[4] Bhat, S.S. and Govardhan, R.N. (2013). Stall flutter of NACA 0012 airfoil at low Reynolds numbers, *Journal of Fluids and Structures*, vol. 41, pp. 166-174.

[5] Gageik, M., Klioutchnikov, I. and Olivier, H. (2015). Comprehensive mesh study for a direct numerical simulation of the transonic flow at Re_c = 500,000 around a NACA 0012 airfoil, *Computers and Fluids*, vol. 122, pp. 153-164.

[6] Rainbird, J.M., Peiró, J. and Graham, J.M.R. (2015). Blockage-tolerant wind tunnel measurements for a NACA 0012 at high angles of attack, *Journal of Wind Engineering and Industrial Aerodynamics*, vol. 145, pp. 209-218.

[7] Katkhaw, N., Vorayos, N., Kiatsiriroat, T., Khunatorn, Y., Bunturat, D. and Nuntaphan, A. (2014). Heat transfer behavior of flat plate having 45° ellipsoidal dimpled surfaces, *Case Studies in Thermal Engineering*, vol. 2, pp. 67-74.

[8] Siauw, W.L., Bonnet, J.-P., Tensi, J., Cordier, L., Noack, B.R. and Cattafesta, L. (2010). Transient dynamics of the flow around a NACA 0015 airfoil using fluidic vortex generators, *International Journal of Heat and Fluid Flow*, vol. 31, pp. 450-459.

[9] Liang, Z.-C. and Xue, L.-P. (2014). Detached-eddy simulation of wing-tip vortex in the near field of NACA 0015 airfoil, *Journal of Hydrodynamics*, vol. 26(2), pp. 199-206.

[10] Šidlof, P., Vlček, V. and Štěpán, M. (2016). Experimental investigation of flow-induced vibration of a pitch–plunge NACA 0015 airfoil under deep dynamic stall, *Journal of Fluids and Structures*, vol. 67, pp. 4859.

[11] Haocheng, F., Mingqiang, L., Hu, L. and Zhe, W. (2011). A Knowledge-based and extensible aircraft conceptual design environment, *Chinese Journal of Aeronautics*, vol. 24, pp. 709-719.

[12] UIUC Applied Aerodynamics Group (2016). *UIUC Airfoil Coordinates Database*, URL: http://m-selig.ae.illinois.edu/ads/coord_database.html#C, accessed on 1/11/2016

[13] Drela, M. and Youngren, H. (2013). *Xfoil Subsonic Airfoil Development System*, URL: http://web.mit.edu/drela/Public/web/xfoil, accessed on 1/11/2016

[14] Le, N.T.P., Shoja-Sani, A. and Roohi, E. (2015). Rarefied gas flow simulations of NACA 0012 airfoil and sharp 25–55-deg biconic subject to high order nonequilibrium boundary conditions in CFD, *Aerospace Science and Technology*, vol. 41, pp. 274-288.

[15] Launder, B.E. and Sharma, B.I. (1974). Application of the energy-dissipation model of turbulence to the calculation of flow near a spinning disc, *Letters in Heat and Mass Transfer*, vol. 1, pp. 131-138.

[16] Patankar, S.V. (1980). Numerical Heat Transfer and Fluid Flow, McGraw-Hill Book Company, New York.

[17] *Reynolds number calculator*, URL: http://airfoiltools.com/calculator/reynoldsnumber, accessed on 1/11/2016

[18] Munson, B.R., Young, D.F., Okiishi, T.H. and Huebsch, W.W. (2010). Fundamentals of Fluid Mechanics, John Wiley & Sons, Asia.